





Article

Landslide Susceptibility Mapping for Austria Using Geons and Optimization with the Dempster-Shafer Theory

Thimmaiah Gudiyangada Nachappa ^{1,*}, Sepideh Tavakkoli Piralilou ¹,
Omid Ghorbanzadeh ¹, Hejar Shahabi ² and Thomas Blaschke ¹

¹ Department of Geoinformatics—Z_GIS, University of Salzburg, 5020 Salzburg, Austria; sepideh.tavakkoli-piralilou@stud.sbg.ac.at (S.T.P.); omid.ghorbanzadeh@stud.sbg.ac.at (O.G.); thomas.blaschke@sbg.ac.at (T.B.)

² Department of Remote Sensing and GIS, University of Tabriz, Tabriz 5166616471, Iran; h.shahabi94@ms.tabrizu.ac.ir

* Correspondence: thimmaiah.gudiyangadanachappa@sbg.ac.at

Received: 31 October 2019; Accepted: 6 December 2019; Published: 10 December 2019



Abstract: Landslide susceptibility mapping (LSM) can serve as a basis for analyzing and assessing the degree of landslide susceptibility in a region. This study uses the object-based geons aggregation model to map landslide susceptibility for all of Austria and evaluates whether an additional implementation of the Dempster–Shafer theory (DST) could improve the results. For the whole of Austria, we used nine conditioning factors: elevation, slope, aspect, land cover, rainfall, distance to drainage, distance to faults, distance to roads, and lithology, and assessed the performance and accuracy of the model using the area under the curve (AUC) for the receiver operating characteristics (ROC). We used three scale parameters for the geons model to evaluate the impact of the scale parameter on the performance of LSM. The results were similar for the three scale parameters. Applying the Dempster–Shafer theory could significantly improve the results of the object-based geons model. The accuracy of the DST-derived LSM for Austria improved and the respective AUC value increased from 0.84 to 0.93. The resulting LSMs from the geons model provide meaningful units independent of administrative boundaries, which can be beneficial to planners and policymakers.

Keywords: landslide susceptibility mapping; geons; Dempster–Shafer theory; object-based; natural hazards

1. Introduction

Natural hazards worldwide are increasingly causing the loss of lives and resulting in increasing economic losses [1]. Landslides are one of the most common and prominently occurring natural hazards in mountainous regions, impacting human lives and infrastructure and causing economic loss [2]. A landslide is defined as the gravitational movement of a mass of rock or debris down a slope [3]. In general, landslides are mass movements that include rock falls, mudslides, and debris flows. Classifications of landslides are usually based on the material, such as rock, debris, earth, or mud; and the movement type, such as fall, topple, avalanche, slide, flow, or spread. Triggering factors for landslides can be natural processes, such as heavy and prolonged precipitation, earthquakes, rapid snowmelt, and permafrost thawing; or human-made factors, such as the construction of roads, buildings, irrigation, or combinations of natural and human-made triggers [4]. The occurrence of landslides is likely to increase in the future due to the impact of human activities, population growth, infrastructure development, and mistreatment of natural resources. Landslides can, in principle, be considered natural phenomena, but they are often triggered by the impact of human undertakings [5].

With the increasing impacts of landslides worldwide, a substantial increase in scientific research on landslides can also be observed [6]. Especially Europe witnessed a substantial increase in mortalities and economic losses from natural hazards, which were mainly landslides. These landslides occurred as a result of physical, geological, meteorological, morphological, and anthropogenic factors [7]. To comprehend and study the influence of landslides on human and economic losses, it is essential to study a region's susceptibility to landslides. Landslide susceptibility is the potential impact of a particular type of landslide on a specific area in the future [8]. Landslide susceptibility mapping (LSM) is the spatially explicit quantification of the probability of the occurrence of landslides in the future based on the effects of conditioning factors in the given area [9]. A susceptibility map identifies areas within the study region that are more or less prone to landslides in the future based on relatively higher or lower probabilities or classes of probabilities [10]. The LSM is decisive in the management of landslides, and various methods have been used to analyze landslide susceptibility [11,12]. LSM aims to quantify, map, and ultimately understand the spatial distribution of landslide occurrences in the future [13]. Although susceptibilities to certain other types of natural hazards may be easier or more exact to model and map (e.g., floods), landslide susceptibilities are an effective and widespread planning tool [14]. Many previous studies target the landslide susceptibility at a regional level or for a single watershed, while research at a national scale is rare [15].

The advancement in technologies such as geographic information systems (GIS) and remote sensing (RS) have considerably assisted in enhancing planning and mitigating future natural catastrophic events [16]. There are various methods for extracting information from images through GIS and RS. The object-based extraction of information for landslide susceptibility has been predominant in recent years [17]. Most of the LSM has been carried out using either a pixel-based, data-driven approach or an expert-based approach. Various methods are being used for LSM, such as the data-driven frequency ratio (FR) [18–20], expert-based analytical hierarchical process (AHP) [21,22], evidence belief function (EBF) [23], machine learning models of support vector machines (SVM) [24], random forest (RF) [25], and logistic regression (LR) [26,27].

During the past two decades, object-based image analysis (OBIA) has developed as an extension of Geographic Information Science (GIScience) and is used to analyze and process very high-resolution satellite imagery [28]. OBIA builds on image analysis, which is an older concept similar to image segmentation and image classification. The object-based classification presents a viable alternative to the pixel-based approach [29]. The image segmentation process is a crucial prerequisite for classification [30] and further analysis in the so-called geons approach.

Geons are spatial units that are “homogenous in terms of varying space and time phenomena under policy concern” [31]. This geons model incorporates expert knowledge and semi-automatically delineates regions. The method will be explained in greater detail in Section 3.3.1. The resulting landslide susceptibility maps are highly dependent on the input data, namely the landslide inventory and the influencing conditioning factors relevant to the study area. The study of LSM at a national scale has been carried out for the first time using an object-based geons model along with nine conditioning factors relevant to the study area. The overall aim is to use geons for the LSM, utilize the DST to optimize the resulting LSMs from multi scales, and reduce the associated uncertainty.

The image segmentation approach can affect the accuracy of the classification and has a considerable influence on the resulting LSMs. An incorrect segmentation usually results in over-segmentation and under segmentation errors [32]. Thus, finding the optimal parameters for the segmentation process plays an essential role in LSM using geons. The optimum scale parameter (SP) must be considered for the process of finding the appropriate segments for the susceptibility analyses [33]. Although there is never an ideal solution to the segmentation process, this process can lead to better results when using the optimal SP [34]. Although some landslide conditioning factors are prepared from RS data with a similar spatial resolution (e.g., the slope and elevation), there are some factors with different resolutions (e.g., rainfall and lithology) that are generated from different sources. Thus, all the LSM is done within a multiresolution and multiscale environment [35]. Therefore, an optimal scale-out of multiple

scales can be found for the LSM with less internal heterogeneity compared to the adjacent areas [36]. The optimal SP for segmenting our data was obtained by applying the estimation of scale parameters (ESP2) tool [33]. Multiscale were chosen using interval values based on the optimal SP. The resulting LSMs from multiscale segmentation and geons were then fused using Dempster–Shafer theory (DST) to show the higher performance of susceptibility map generation in a multiscale environment. The DST, which is also known as evidence theory, is principally based on representing independent sections of evidence by completely monotone capacities (also known as belief functions), and pooling them by means of a common operator called Dempster’s rule of combination [37]. This probability method has been used to optimize the results of various natural hazard susceptibility mapping projects [38–40].

In this study, we use the OBIA-based aggregation approach of “geons” for the LSM of Austria. In Austria, landslides are a significant natural hazard in alpine and mountainous areas. We investigate the conditioning factors, such as lithology, geology, land cover, and geomorphology (primarily slope angle and aspect), and produce LSM for the whole territory. This is of high importance because recent landslide events in Austria have caused severe mortalities, as well as high economic losses.

2. Study Area

Austria is situated in the center of the European continent, covering an area of 83,858 km² and is home to approximately 8.8 million inhabitants. The elevation ranges from 110 m to 3800 m. Due to the geomorphological setting of Austria, landslides occur quite frequently in most parts of the country that are not flat, and they pose a serious threat to infrastructure and public property [41]. The mountainous areas are prone to the large mass movement, rockfalls, and landslides, causing damage to infrastructure and loss of lives. In Austria, the mean annual rainfall ranges from 400 to 600 mm per year in the flat or hilly eastern regions, while the mean annual rainfall exceeds 2000 mm per year in alpine areas. Austria was selected as the study area as there has never been a study on landslide susceptibility mapping at the national scale using an object-based model. Ten GIS-based thematic layers of factors that contribute to landslides were selected for the geon-based LSM. The thematic layers used were elevation, slope, aspect, geology, lithology, rainfall, land cover, distance to roads, distance to faults, and distance to drainage. Figure 1 shows the study area and landslide inventory data.

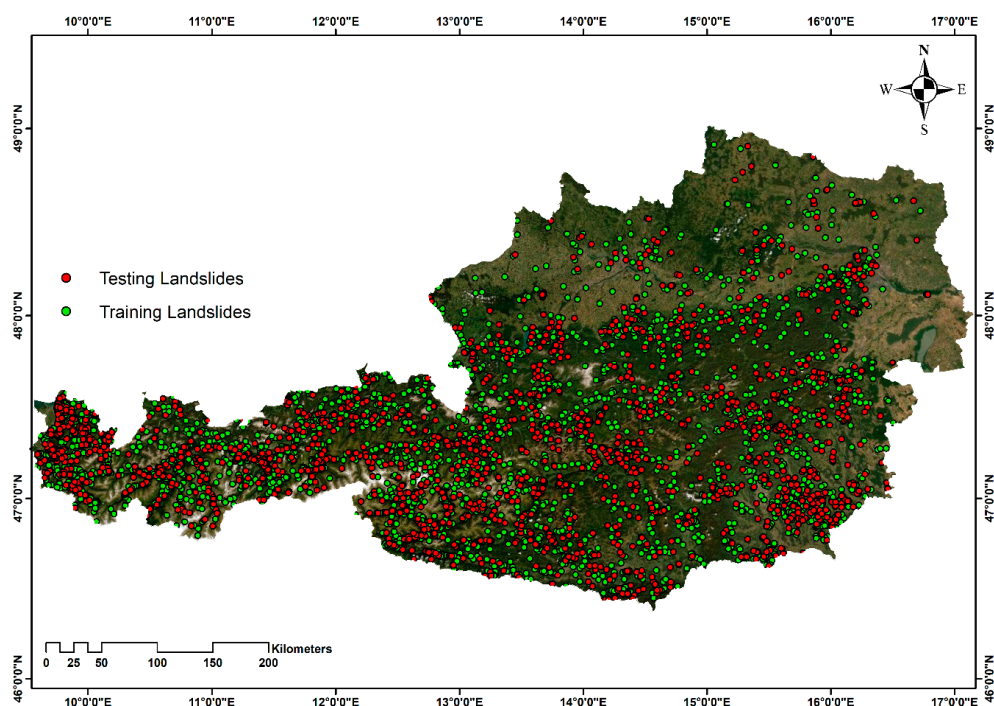


Figure 1. Map of Austria with dots from the national landslide inventory, divided into training and testing landslides.

3. Materials and Methods

3.1. Landslide Inventory Data

Landslide inventory data for Austria was provided by the Geological Survey of Austria (GBA) on April 11, 2019 and contains 6309 landslide point features. The landslide inventory data is not updated continuously, nor is it a complete dataset for Austria. For the analysis, the landslide inventory was divided into training and validation data. As there is no authoritative standard for dividing inventory data into training and validation data sets [42], the most common approach in literature was used to classify the inventory data, namely 70/30. This means the inventory points were randomly divided into two groups: 70% (4416) for training and 30% (1893) for validation. Figure 1 shows the training and testing of landslide inventory data used for the study area.

3.2. Landslide Conditioning Factors

In general, there are no predefined criteria for selecting conditioning factors for landslide susceptibility. The selected factors should be operative, quantifiable, non-uniform, and non-redundant [43]. Based on the national geomorphological characteristics and previous studies, nine conditioning factors were selected for this LSM. The nine conditioning factors are elevation, slope, aspect, lithology, rainfall, land cover, distance to roads, distance to faults, and distance to drainage. The digital elevation model (DEM) with 10 m resolution was obtained through open data for Austria, and slope and aspect layers were derived from the DEM. Land cover data were obtained from the Austrian Land Information System (LISA). Lithology and fault data were obtained from the Geological Survey of Austria (GBA). The drainage and road network data were obtained from the open street map (OSM) Humanitarian OpenStreetMap Team (HOT) data export tool. Rainfall data were obtained from Klimaszenarien für Österreich (ÖKS15) for Austria. All the mentioned data was processed to 10 m resolution to produce landslide conditioning factors using Environmental Systems Research Institute (ESRI) maintained ArcGIS software. Figure 2 shows the landslide conditioning factors used in this study.

The elevation is a key conditioning factor. Three out of the nine conditioning factors are direct measures (elevation) or are directly influenced by elevation (slope and aspect) [44]. Elevation influences other topographic attributes of a region that can lead to spatial variabilities, such as the vegetation distribution. Vegetation changes are directly correlated to the increase in elevation. In this study, elevation was classified into five classes: 0–500 m, 500–1000 m, 1000–1500 m, 1500–2000 m, and > 2000 m above mean sea level.

The slope angle directly affects the stability of the slope. The slope is directly related to landslides, as a greater angle of slope is more susceptible to failure [35]. The slope angle conditioning factor was derived from the DEM and classified into five classes: 0°–10°, 10°–20°, 20°–30°, 30°–40°, and > 40°.

The slope aspect influences the slope steadiness indirectly through the hydrologic process, such as rainfall, and also influences the weathering process [2]. The aspect defines the slope direction. Slope aspect was categorized into nine classes: north (0°–22.5°; 337.5°–360°), northeast (22.5°–67.5°), east (67.5°–112.5°), southeast (112.5°–157.5°), south (157.5°–202.5°), southwest (202.5°–247.5°), west (247.5°–292.5°), northwest (292.5°–337.5°), and flat (0°).

In many studies, lithology has been recognized as one of the key conditioning factors for LSM. Lithological units vary based on their strength, permeability, and susceptibility to failure [45]. A variation of lithological units may mean a variation of strength and permeability within the rock strata. The lithological units of Austria were classified into 23 main classes: orthogneiss, gneiss, paragneiss, granite, gravel, amphibolite, marble, limestone, metasediment, sandstone, carbonate rock, coarse clastics, mica schist, phyllite, volcanic rock, andesite, ophiolite, serpentinite, calcitic marble, tonalite, eklogite, dolomite, and water.

Land cover is another key conditioning factor for LSM [46,47]. Aside from the topography, land cover can often explain highly complex landslide patterns in the resulting LSMs. Land cover data were

classified into ten classes: built-up, flat sealed surfaces, permanent soil, bare rock and scree, water, snow and ice, trees, bushes and shrubs, herbaceous, and reeds.

In Austria—as earthquakes are relatively rare—rainfall is the main triggering factor for landslides and a critical factor in LSM. Rainfall features can vary by weather situations and topographical features, which can cause substantial temporal and spatial variances in a rainfall event. Annual precipitation data were classified into four classes: 0–600 mm, 600–1200 mm, 1200–1800 mm, and >1800 mm.

Distance to drainage is a hydrological process of slope that influences LSM: the closer to drainage, the more erosion. Drainage delivers water that causes material saturation, resulting in landslides into the valley [48]. The study area was classified into five classes, namely the intervals of 0–500 m, 500–1000 m, 1000–1500 m, 1500–2000 m, and >2000 m.

Distance to roads is a crucial anthropogenic factor for the occurrence of landslides [49]. The distances to roads were classified into the five buffer zone classes of 0–200 m, 200–400 m, 400–600 m, 600–800 m, and >800 m.

Active faults play a significant role in landslides [50]. Firstly, they are the source of occurrences of earthquakes, and secondly, active faults have vital roles in cracking of stones, which in turn creates instability. This disjointed formation of geology leads to reductions in the shear resistance of the rock strength and triggers the occurrence of landslides. The distance to faults was classified based on the distance of landslides (Euclidean distance) from the fault and classified into the following five classes: 0–1000 m, 1000–2000 m, 2000–3000 m, 3000–4000 m, and >4000 m distances.

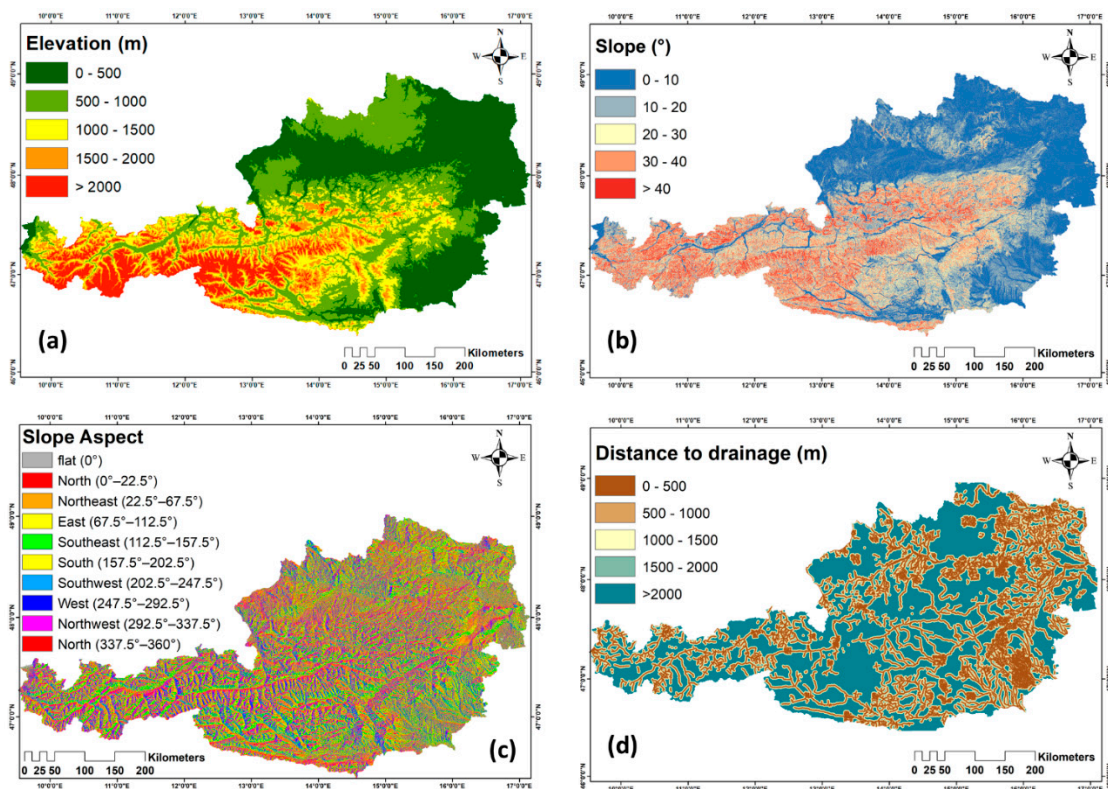


Figure 2. Cont.

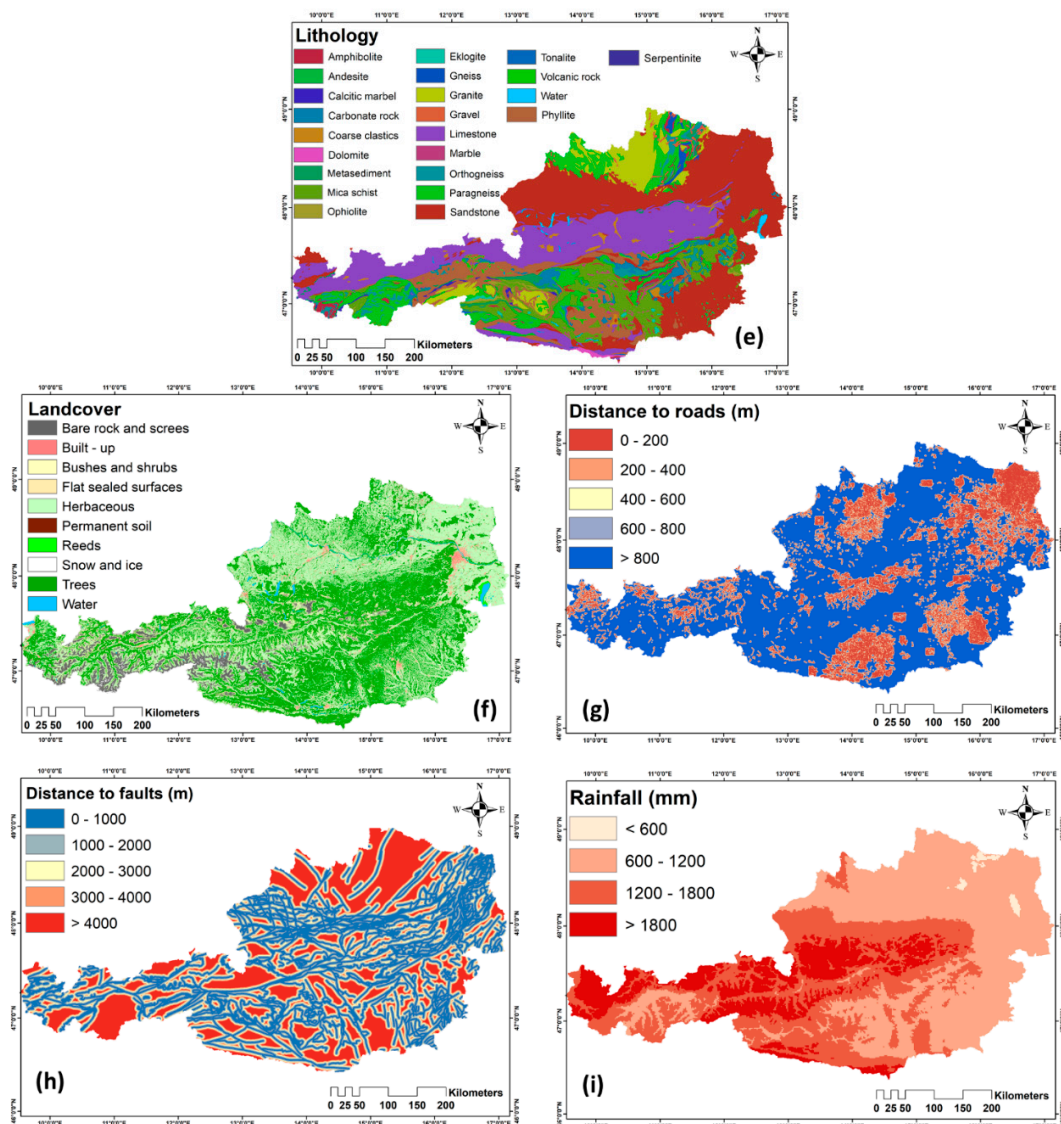


Figure 2. Landslide conditioning factors: (a) elevation (m); (b) slope; (c) aspect; (d) distance to drainage (m); (e) lithology; (f) land cover; (g) distance to roads (m); (h) distance to faults (m); (i) rainfall.

3.3. Methodology

The landslide susceptibility analysis was based on an object-based geons aggregation model for Austria. We chose the geons aggregation model as it had not previously been used for landslide susceptibility analysis, meaning this is the first time that this model has been implemented for all of Austria. The weights for the geons model can be derived from data-driven or expert-based approaches. The expert-based approach is based on multicriteria decision analysis, such as the analytical hierarchical process. For the weighting, we chose the multi criteria-based weights derived from experts and used these as the inputs for the geons model. Figure 3 shows the overall workflow of the process followed and the methodologies used for the landslide susceptibility mapping.

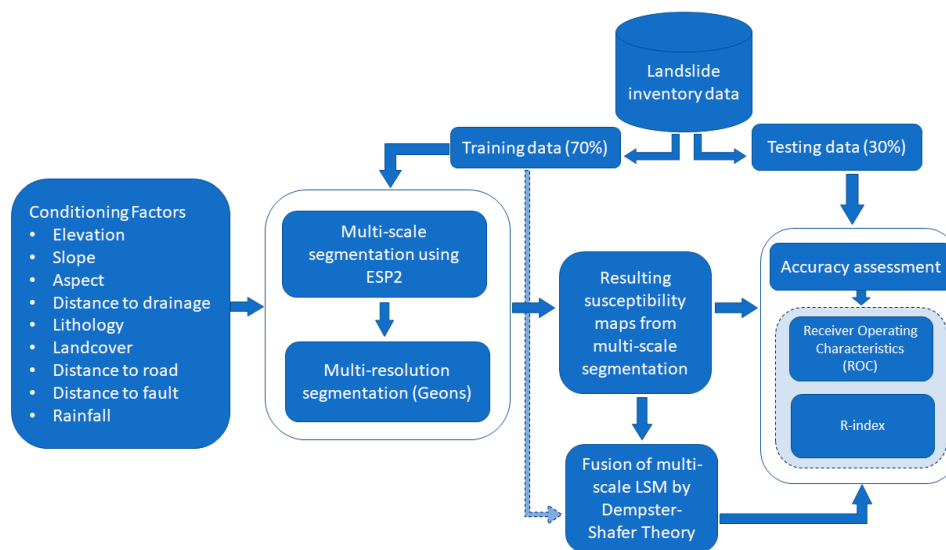


Figure 3. Workflow of the applied methodology. Note: LSM = landslide susceptibility mapping; ESP2 = estimation of scale parameters.

3.3.1. Geons

Lang et al. [31] introduced the geons concept as aggregate units that have their own meaning and representativeness. Geons are, therefore, not the smallest possible geometric entities, and they are purpose-driven. Geons are closely related to object-based image analysis (OBIA) and object-based classification. The latter—with or without images as constituent parts—seems to be well suited for mimicking the subjectivity of visual interpretation in digital classification. Walter and Fritsch proposed an object-based classification on the basis that human vision can differentiate the thematic objects through groups of image pixels [51]. The object-based classification has been increasingly used for high-resolution classification [52]. Geons are well-defined as spatial units that are homogenous in terms of varying space and time phenomena under policy concern [31]. A geon is a type of region that is semi-automatically delineated using expert knowledge. The main aim of generating geons is to map policy-relevant spatial occurrences using an adaptive and expert-validated method to visualize and help to understand the spatial distribution to improve planning and evaluation measures for intervention [17]. Geons are scale-specific spatial objects with steadiness features, such as reduced inherent variance and gradients toward the outside through vector encoding [31,53]. A geons model works as a two-step process, where the first step is based on domain-specific expert knowledge, and the second is based on semi-automated regionalization through segmentation [54]. Object-based image analysis (OBIA) has various algorithms for segmentation. Multiresolution segmentation is a commonly used algorithm for the segmentation of images into image objects [52]. Multiresolution segmentation (MRS) creates homogenous image segments through scale representations. To minimize the loss of detail during the segmentation, aggregation of spectral information is carried out in a scale-adaptive manner. The MRS process starts aggregating from the pixel level and then aggregates into objects of varying shapes and sizes until the preset threshold is reached. The key issue with MRS is the selection of key parameters, especially the scale parameter (SP). To select the optimal scale parameter for the analysis the Estimation of Scale Parameter tool (ESP) was developed, which detects the optimal scale based on the local variance graph using a single layer [55]. This ESP tool was extended to ESP2, which is an automated method for the selection of the optimal scale parameter that provides three distinct scales using multiresolution segmentation. The geons model was entirely processed in eCognition (Trimble) software in combination with the ESP2 tool, which operates within the eCognition software environment and aims to obtain statistically significant scale parameters. The output of the ESP2 tool is three scale parameters. In this study, these parameters determine the SP of the input conditioning factors, and we used the finest scale parameter for the geons model. Lastly, all nine conditioning

factor layers were converted to GeoTIFF (georeferenced information embedded within a Tagged Image File Format) files, with normalized values ranging from 0–255 and 8-bit unsigned integer values for implementing geons in the eCognition software.

3.3.2. Dempster–Shafer Theory (DST)

The concept of DST is based on a frame of discernment and is known as a belief function (Bel) that is derived from the Bayesian probability theory (BPT), which identifies this algorithm as a soft classifier. However, the difference between BPT and DST is that the priors and conditionals need not be specified and the basic assumption of DST is that ignorance exists instead of supplying prior probabilities [56]. The name DST is obtained from the extensions and clarifications presented by Shafer. The DST is considered as a useful approach to integrating spatial data and can provide a mathematical framework for the description of incomplete knowledge [57]. Moreover, the DST is well known as evidence theory, which defines basic probability assignment (bpa) functions to provide a combination of evidence [58]. It defines hypotheses in a hierarchical structure developed from a basic set of hypotheses that form the framework of discernment [59]. The DST is an effective method for modelling imprecision and uncertainty assessment, and it can provide additional flexibility for the specification of uncertainty in probabilistic models and hypothesis testing. DST has mostly been applied with a focus on uncertain reasoning in artificial intelligence and expert systems. In this theory, displaying information requires two essential functions, namely the Bel and plausibility function (Pl), from which the lower bound value for a (known) probability function and the upper bound for a probability function (an unknown probability function) are derived, respectively. The differentiation between Bel and Pl illustrates the uncertainty of the knowledge about the objective proposition [60].

The DST provides an extension of the probability framework for assessing the uncertainty of any imprecision event of the probability $P(M_l)$ that the alternative method $M_l, l = 1, \dots, n$ is correct. The lower bound indicates the degree of knowledge or belief that supports M_l and represented by $Bel(M_l)$, whereas the upper bound contributes to M_l and is called plausibility $Pl(M_l)$ [61] (see Equations (1) and (2))

$$Bel(A) = \sum_{B \subseteq A} m(B) \tag{1}$$

$$Pl(A) = \sum_{B \cap A \neq \emptyset} m(B) \tag{2}$$

where the summation is taken over all sets $B \in 2\theta$ with $B \subseteq A$ in the definition of Bel and the summation in that of Pl is taken over all sets $B \in 2\theta$ with $B \cap A \neq \emptyset$, for which the set of θ is a mutually exclusive and collectively exhaustive hypothesis, and the power set of θ is denoted by 2θ . The Bel is the summation of all masses directly assigned to that by a set of hypothesis A , while the plausibility sums all masses not assigned to the complement of hypothesis A . An uncertainty interval is defined as $Bel(A), Pl(A)$ and has the following properties:

$$Bel(A) \leq Pl(A)$$

$$Pl(A) = 1 - Bel(\bar{A})$$

where \bar{A} is the negation of A and $Bel(\bar{A})$ is called the disbelief function. These properties indicate that the unknown true probability lies somewhere between the belief and plausibility functions. The difference between these two functions, which is called the belief interval or ignorance, represents the ignorance of one's belief of the target proposition A and can be regarded as a measure of the imprecision of knowledge about the uncertainty of set A [62]. This belief interval or ignorance is the main distinguishing feature of the DST of evidence compared to the traditional probability theory. From the general point of view, unlike a probabilistic theory that allocates a mass to the individual elementary events, the theory of evidence, or the bpa, makes $m(A)$ on set A of the $P(z)$, the power sets of space Z event (i.e., on a set of results rather than a single elementary event).

In more detail, $m(A)$ expresses the degree of belief that a specific element x belongs to set A only, and not to any subset of A . The bpa that assigns a mass in the range of $[0, 1]$ to each subset A satisfies the following requirement in Equation (3):

$$m : P(Z) \rightarrow [0, 1], m(\varnothing) = 0; \sum_{A \in Z} m(A) = 1 \tag{3}$$

If n data sources are available, probability masses $m_i(B_j)$ have to be defined for each data source i with $1 \leq i \leq n$, and for all sets $B_j \in \theta$. The DST allows the combination of these probability masses from resulting landslide detection maps and from the training inventory data set to compute a combined probability mass for each set. The composition rule in the proposed DST is based on mathematical theory, which is the basis of the combination of mass functions m_i obtained from n sources of information given in Equations (4) and (5):

$$m(A) = m_1(B_1) \oplus m_2(B_2) \oplus m_3(B_3) \dots \oplus m_n(B_n) \tag{4}$$

$$m(A) = \frac{\sum_{B_1 \cap B_2 \dots B_n = A} \prod_{i=1}^n m_i(B_j)}{(1 - K)} \tag{5}$$

where K denotes the degree of conflict given in Equation (6):

$$K = \sum_{B_1 \cap B_2 \dots B_n = \varnothing} \prod_{i=1}^n m_i(B_j) \tag{6}$$

3.3.3. Fusion of Multiscale Results Via DST

Multiscale segmentation results in different object sizes, which are used for geons models. Thus, based on multiscale segmentation, different LSMs were produced using the geons model. The areas that were classified as landslides using three different scales were grouped using the fusion level analysis technique [38] and fused into a class of landslide area based on the DST. In the inventory dataset, the landslide points were transferred to the corresponding pixels. Therefore, the DST process considered the area of each pixel. The resulting LSMs from the three different scales were classified using the natural break classification technique into five susceptibility categories, namely very low, low, moderate, high, and very high. Then, to apply DST, all five categories were converted into two classes, either zero and one, whereby class zero contained the very low, low, and moderate categories, while class one contained high and very high susceptibility categories. The result was a binary map of zero and one.

Several Bels were combined in the DST within the same framework, making it possible to harmonize the landslide-susceptible (LS) areas from different scales. The probability of uncertainty in the LS areas can be derived from Bel and Pl. Therefore, the resulting LS areas of three scales (1300, 1500, 1700) were combined by fusing the DST with only the training inventory dataset. The accuracy of the landslide-detected areas based on each scale was assessed using a confusion matrix, and accordingly, the Bels were estimated with a precision function [38]. The DST combined the majority of LS areas, which are closer to the inventory dataset, and then assigned them into the class of landslide area based on the DST. The resulting LSM based on the DST was then converted to the same number of five classes using the natural break classification technique.

4. Results

4.1. Geons

The resulting LSMs were generated using the geons model to identify the regions susceptible to landslides in Austria. Weights for each conditioning factor were based on expert knowledge and were used for multiresolution segmentation. The resulting maps were classified based on the quantile classification technique, which is a commonly used classification technique for natural hazard susceptibility mapping. The results were classified into five categories: very low, low, moderate, high,

and very high. Figure 4 shows the LSM map derived from geons considering the optimal SP of 1500, and Figure 5 shows the LSM from geons with regions.

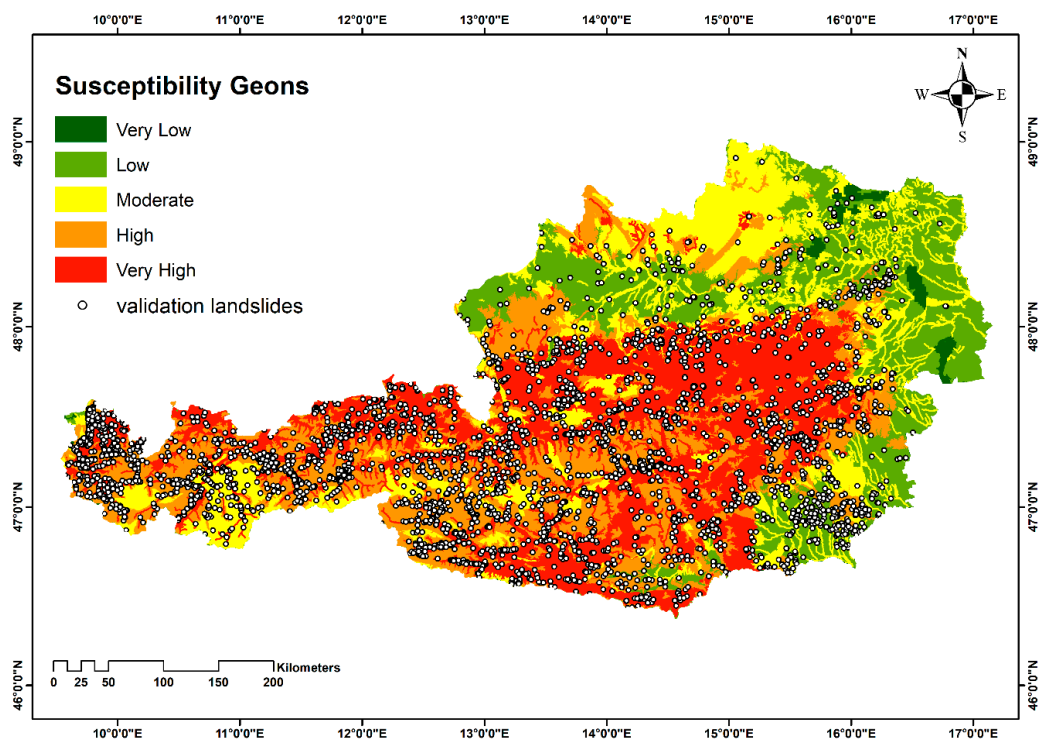


Figure 4. The LSM derived from geons using the optimal scale parameter (SP) of 1500 and the validation landslide locations.

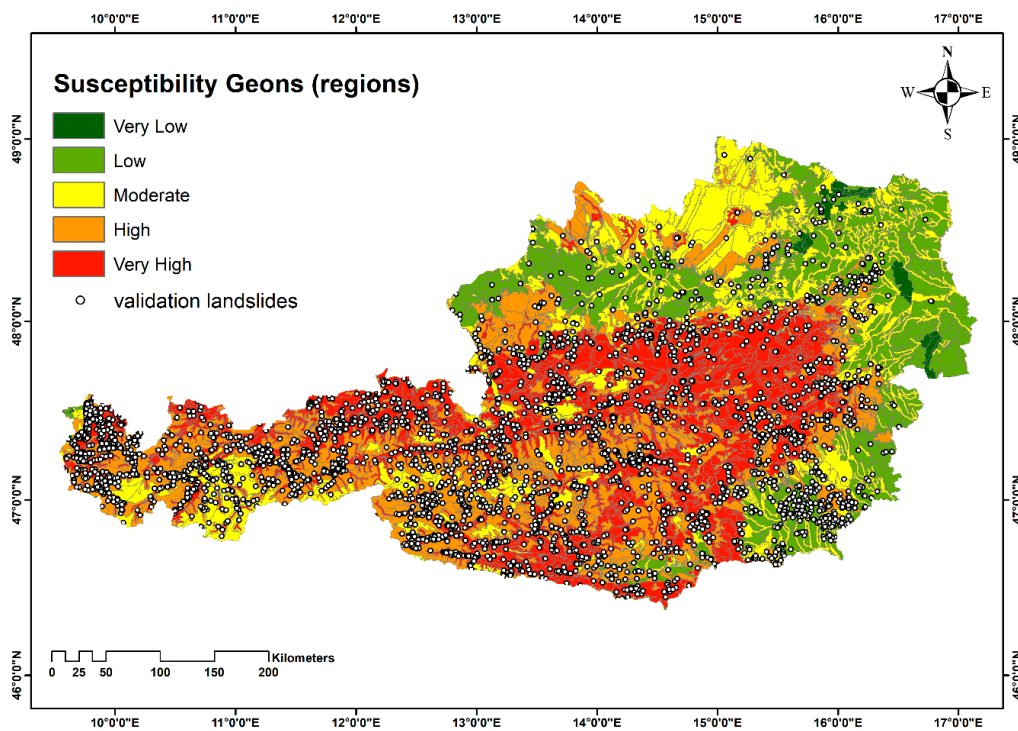


Figure 5. The LSM derived from geons using the optimal SP of 1500, showing the regions and the validation landslide locations.

For a better understanding of how each conditioning factor influenced the final LSM derived from the geons model, we show the susceptibility classes of the areas categorized into five classes.

The advantage of the geons model is that it shows how each region (geon) has been characterized, and the impact of each conditioning factor on the resulting LSM. We selected four random locations from the derived LSM and visualized the impact of each conditioning factor in these random locations.

Figure 6 shows the four random locations chosen to understand the impact of each conditioning factor on the final landslide susceptibility map using the geons model.

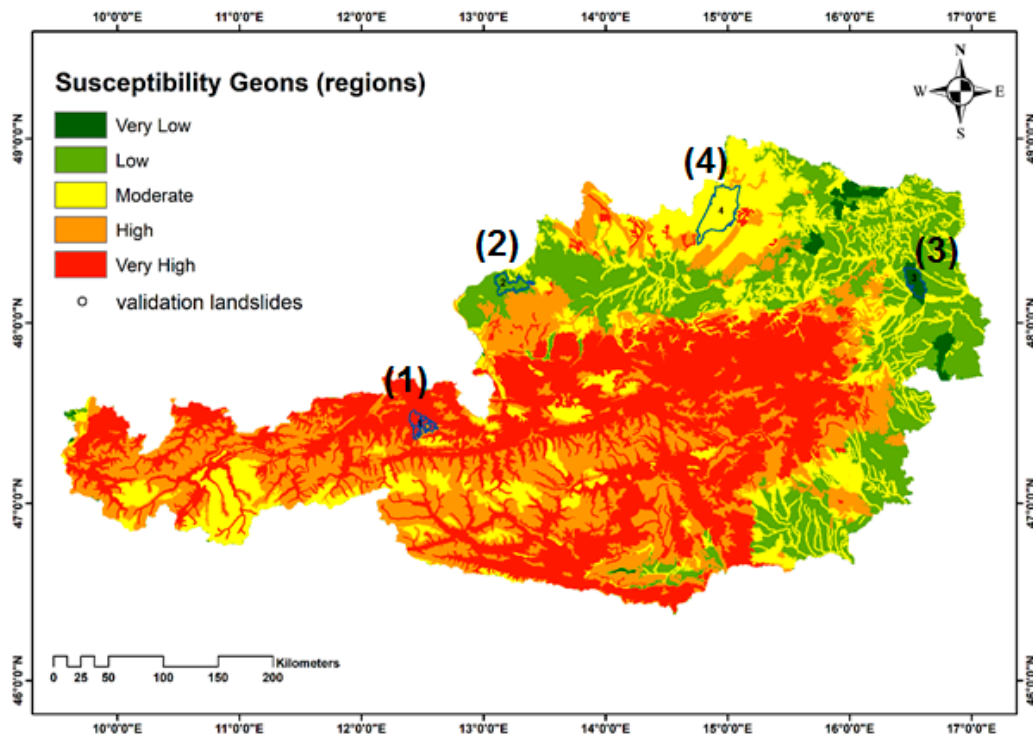


Figure 6. Four locations within the study area were chosen for the impact assessment of each conditioning factor on the final susceptibility map using geons.

Figure 7 depicts the impact of each conditioning factor at location one. At location one, the impact of the rainfall conditioning factor was the highest, followed by elevation and distance to drainage, whereas the distance to roads had the least impact at that location, followed by lithology, land cover, and aspect. In the final susceptibility map, location 1 is classified as having a very high susceptibility to landslides.

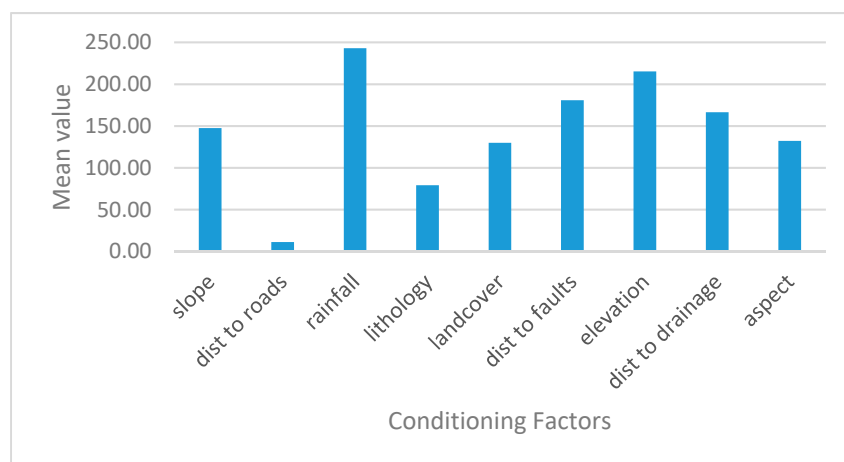


Figure 7. Impact of each conditioning factor at location 1 within the study area.

Figure 8 depicts the impact of each conditioning factor at the second location. At location two, the impact of the distance to the faults conditioning factor was highest, followed by rainfall, whereas

elevation and distance to drainage had no impact at all on the final susceptibility mapping. Factors such as slope and distance to roads had the least or minimal impact on this location. In the final susceptibility map, location 2 falls into the class of low susceptibility.

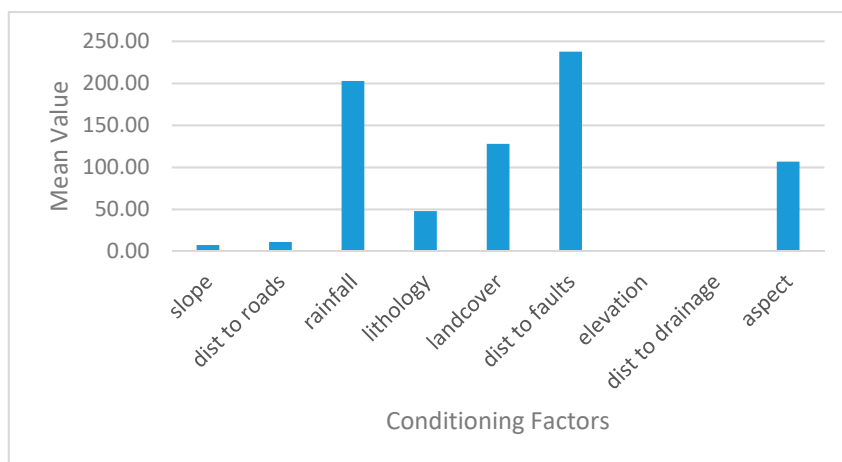


Figure 8. Impact of each conditioning factor at location 2 within the study area.

Figure 9 depicts the impact of each conditioning factor at the third location. Elevation, slope, and rainfall had no impact at all at this location compared to the distance to drainage, which had minimal impact on the final susceptibility map. Distance to faults had a significant impact, followed by land cover, aspect, and distance to roads for the final susceptibility map. In the final susceptibility map, location 3 falls into the very low susceptibility class.

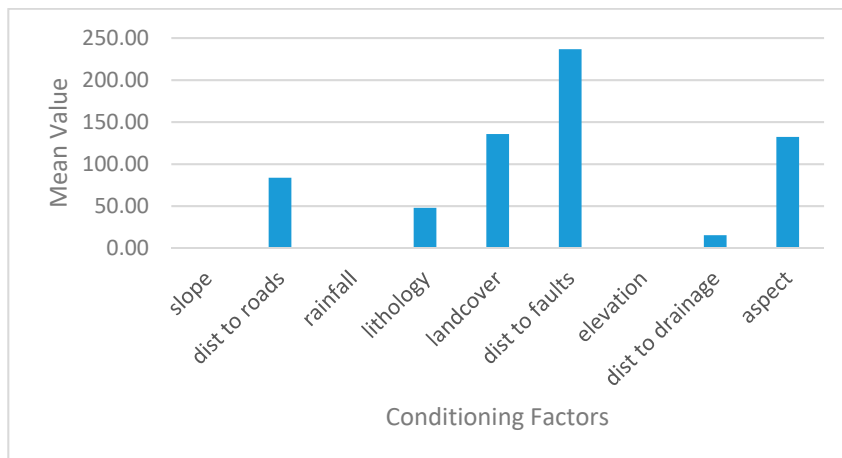


Figure 9. Impact of each conditioning factor at location 3 within the study area.

Figure 10 depicts the impact of each conditioning factor at the fourth location. At location four, distance to roads, distance to faults, and distance to drainage had no impact at all on the final susceptibility map. Slope and lithology had minimal impact on the final susceptibility map, whereas rainfall and elevation had major impacts, followed by land cover and aspect factors. In the final susceptibility map, location 4 falls into the moderate susceptibility category.

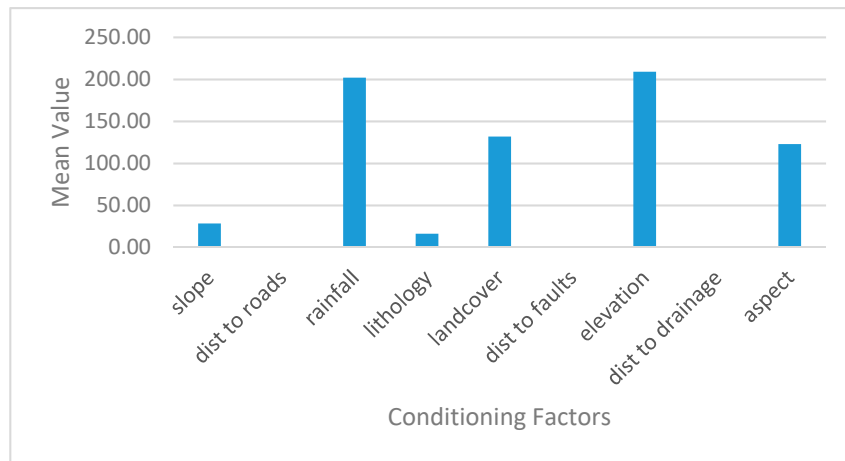


Figure 10. Impact of each conditioning factor at location 4 within the study area.

4.2. Dempster–Shafer

The resulting LSMs of three scales (1300, 1500, and 1700) were combined by fusing the DST with only the training inventory dataset. By comparing the LS areas of each resulting LSM with the inventory dataset, the DST combined the LS areas that were correctly classified within different scales. The resulting DST-based LSM was classified based on the quantile classification technique, which is a commonly used classification technique for natural hazard susceptibility mapping. The results were classified into five categories: very low, low, moderate, high, and very high. Figure 11 shows the optimized LSM using Dempster–Shafer theory based on multiscale segmentation.

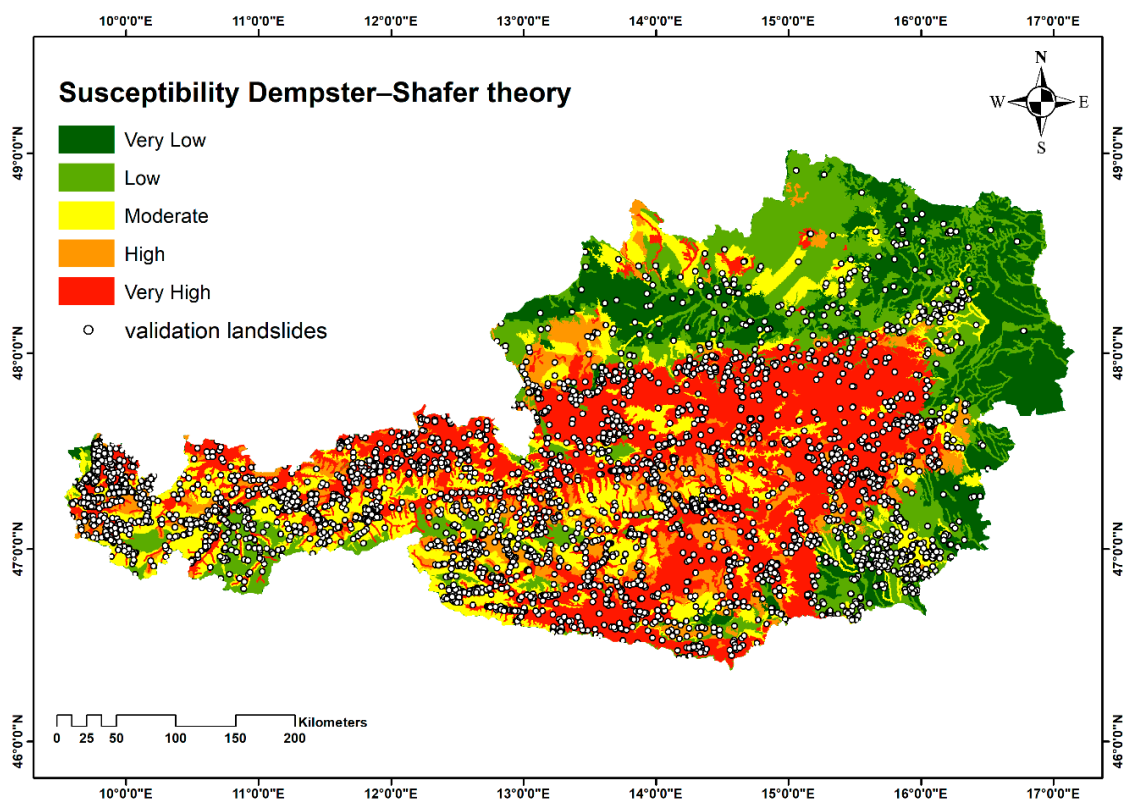


Figure 11. The optimized LSM using Dempster–Shafer theory based on multiscale segmentation.

5. Validation

Validation is a vital part of the analysis because it enables insights into the prediction accuracy of the models [63]. To determine the accuracy of the geons model for the LSM of Austria, we analyzed the resulting map from the geons model. To understand the effectiveness of the model, the conformity between the landslide inventory dataset and the resulting map is crucial. The accuracy results indicate whether the model used can correctly predict the areas that are susceptible to landslides [2]. Our landslide inventory dataset for Austria has 6309 landslide locations, whereby 70% (4416) of the total landslide data points were used to train the geons model, and 30% (1893) were used to validate the resulting LSM.

5.1. Receiver Operating Characteristics (ROC)

The receiver operating characteristics (ROC) curve is used to validate the resulting LSMs from the geons model. The ROC method enables an evaluation of the true positive rate (TPR) and the false positive rate (FPR) in the resulting landslide susceptibility map [64]. The ROC curve was calculated for the geons model. The TPs are the pixels that were correctly classified as landslides, and the FPs are the pixels that were incorrectly classified as landslides [65]. The ROC curve is derived by plotting the TPR against the FPR. The AUC is the degree that stipulates the accuracy of the resulting landslide susceptibility map. The resulting AUC values indicate the probability of the pixels being labelled correctly. A greater AUC value indicates a higher accuracy of the model, whereas a lower AUC value indicates a lower accuracy of the model. The AUC values obtained for three SPs are shown in Figure 12. Figure 12 shows the ROC curve for the geons model using three different scale parameters (1300, 1500, and 1700). The AUC is very similar for all the three scale parameters used in the geons model.

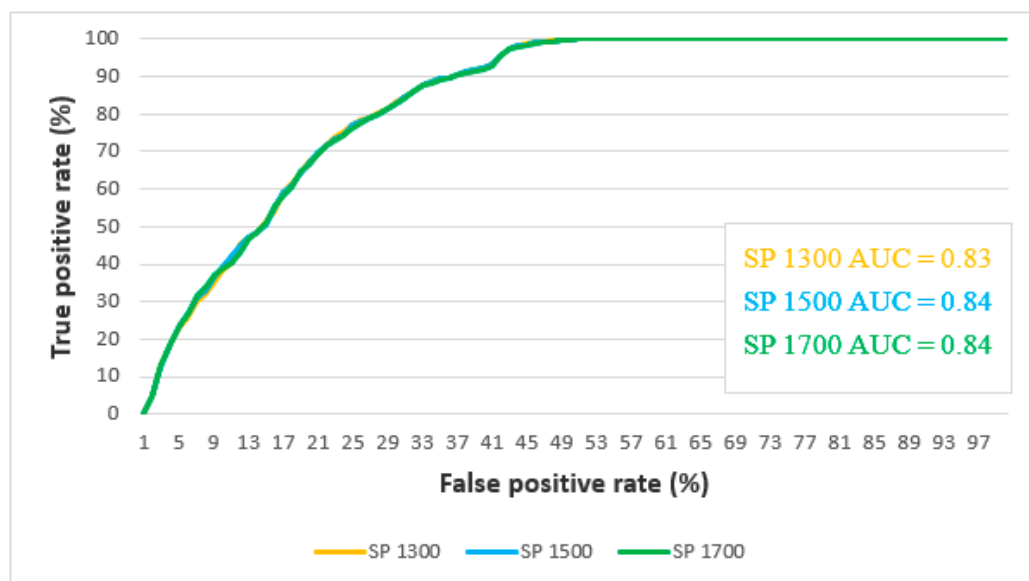


Figure 12. The optimized area under the curve (AUC) values using the geons model for three different scale parameters.

The DST can be used to optimize the overall accuracy of the resulting LSMs. Figure 13 shows the optimized results derived through DST for three scale parameters, along with the DST AUC curve.

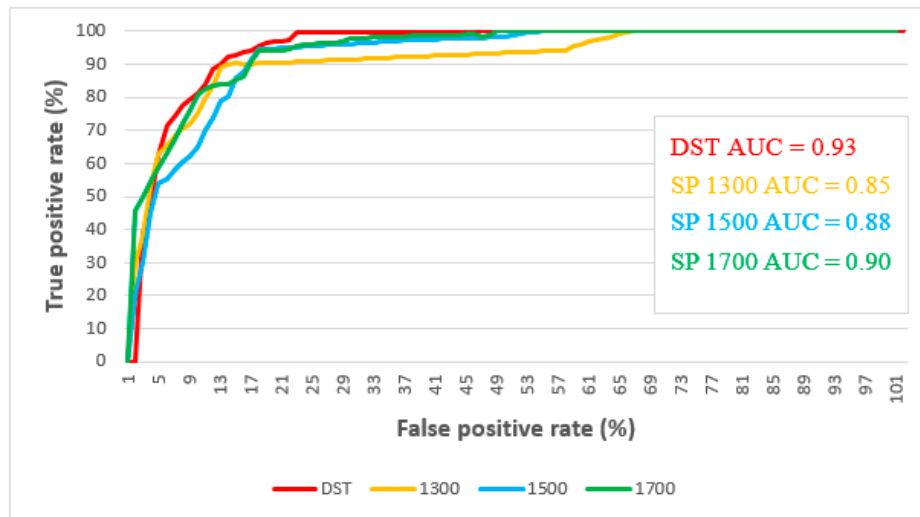


Figure 13. Optimized AUC values using Dempster–Shafer theory (DST) along with three scale parameters.

5.2. Relative Landslide Index (R-Index)

The relative landslide index (R-index) is another validation method for landslide susceptibility mapping. The resulting LSM map from the model is evaluated using the index of relative landslide density. The equation to calculate the R-index is given below

$$R = (n_i/N_i) / \sum(n_i/N_i) \times 100$$

where N_i is the percentage of landslides in each susceptibility class, and n_i is the percentage of the area that is susceptible to landslides in each susceptibility class. The R-index in Table 1 shows the value for five different classes of the resulting landslide susceptibility map and Figure 14 shows the results of R-index plots for the Geons model.

Table 1. R-indexes for the landslide susceptibility mappings (LSMs) of geons.

Validation Methods	Sensitivity Class	Number of Pixels	Area (m ²)	Area Percent (ni)	Number of Landslides	Landslide Percent (Ni)	R-Index
GEONS	Very Low	558,779	2,011,604,400	2.35	5	0.26	3
	Low	4,763,839	17,149,820,400	20.00	110	5.81	8
	Moderate	3,650,614	13,142,210,400	15.32	162	8.56	16
	High	6,577,120	23,677,632,000	27.61	424	22.41	23
	Very high	8,272,806	29,782,101,600	34.73	1191	62.95	50

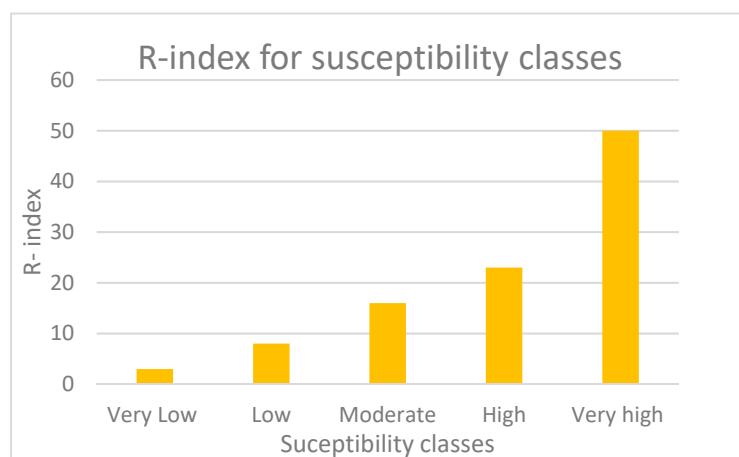


Figure 14. Results of R-index plots for the Geons model.

6. Discussion

The presented research demonstrates the prospect of using an object-based geons model for landslide susceptibility mapping at a national scale. The focal indication of the geons model shows that the susceptible units are independent of any administrative boundaries, thus reducing the biases from artificial borders in the landscape. The advantage of using the geons model is that it allows us to understand the impact of each conditioning factor used in the study area on the final susceptibility map. A proper understanding of the impact of the conditioning factors in each location is crucial for understanding the mechanism of landslide occurrences at a national scale. The results of this study support spatial planners and policymakers in implementing nationwide strategic mapping and mitigation measures based on regions that do not adhere to administrative boundary constraints.

We selected three SPs to study the impact of scale parameters on the object-based geons model and to check whether they have an impact on the accuracy assessments. The results show that the AUC values for the three selected scale parameters are quite similar: results with an SP of 1300 have an AUC of 0.83, those with an SP of 1500 have an AUC of 0.84, and those with an SP of 1700 have an AUC of 0.84, which is similar to that of the SP of 1300. Although generating the LSMs based on multiscale segmentation results in almost the same AUC accuracies, the detected True Positive's (TPs) and False Positive's (FPs) were slightly different. This is why using the DST for the resulting LSMs was advantageous and enhanced the accuracy. The highest increase was detected when using all SPs for the fusion in the DST method. The use of DST to optimize the results of these three SPs showed that this method could be applied for optimization in the LSM.

7. Conclusions

This study produced a nationwide LSM for Austria. The LSM is a key step in the analysis and risk assessment of landslides. The main aim of this study was to evaluate the use of an object-based aggregation model for landslide susceptibility along with meaningful regions, showing the impact of each conditioning factor on the resulting LSM. The resulting susceptibility map for Austria at a national level will help in the planning of landslides countermeasures and help to mitigate the risks in the future. Currently, there is no national-level landslide susceptibility map for Austria that includes all the presented conditioning factors and extends across administrative boundaries. In this research, we utilized the geons model, which is based on object-based classification and provides meaningful regionalized units and is more beneficial than pixel-based approaches. We used the landslide data obtained from the Geological Survey of Austria, which may not be complete. We would like to carry out another assessment in the future with a more comprehensive landslide inventory dataset, ideally provided as areas (polygons) rather than points. The higher accuracy of the geons model showed that the object-based assessment could be successfully implemented for the landslide susceptibility mapping for Austria. The geons model can be adapted for other natural hazard susceptibility assessments and in other regions. The resulting LSM maps can be quite useful for national planners to allocate resources in regions that are more impacted by landslides. Overall, this research presents a landslide susceptibility map for the whole of Austria at a national scale. This study also illustrates that geons allow for meaningful units to be obtained, which is more beneficial for planning purposes than pixels. In our methodology, the effectiveness of using the geons model for LSM is dependent on determining appropriate SPs. Working with multiscale segmentation can result in several different LSMs. Here, the introduced methodology allows for the explicit use of multiple scales, and the DST optimized the resulting susceptibility maps. Our future work will focus on the application of data-driven machine learning models for LSM within an object-based software environment.

Author Contributions: Conceptualization, T.G.N. and O.G.; data curation, T.G.N.; funding acquisition, T.B.; investigation, T.G.N.; methodology, T.G.N., S.T.P., and H.S.; supervision, T.B.; validation, T.G.N.; visualization, T.G.N.; Writing—Original draft, T.G.N. and S.T.P.; Writing—Review and editing, O.G. and T.B. All authors read and approved the final manuscript.

Funding: This research is partly funded by the Open Access Funding of Austrian Science Fund (FWF) through the GIScience Doctoral College (DK W 1237-N23).

Acknowledgments: Authors like to thank Geological Survey of Austria for providing the Landslide inventory data. We also would like to thank autonomous reviewers for their constructive inputs on the manuscript. Open Access Funding by the Austrian Science Fund (FWF).

Conflicts of Interest: The authors declare no conflict of interest.

References

1. Confuorto, P.; Di Martire, D.; Infante, D.; Novellino, A.; Papa, R.; Calcaterra, D.; Ramondini, M. Monitoring of remedial works performance on landslide-affected areas through ground-and satellite-based techniques. *Catena* **2019**, *178*, 77–89. [[CrossRef](#)]
2. Pourghasemi, H.R.; Rahmati, O. Prediction of the landslide susceptibility: Which algorithm, which precision? *Catena* **2018**, *162*, 177–192. [[CrossRef](#)]
3. Clerici, A.; Perego, S.; Tellini, C.; Vescovi, P. A procedure for landslide susceptibility zonation by the conditional analysis method. *Geomorphology* **2002**, *48*, 349–364. [[CrossRef](#)]
4. Wilde, M.; Günther, A.; Reichenbach, P.; Malet, J.-P.; Hervás, J. Pan-European landslide susceptibility mapping: ELSUS Version 2. *J. Maps* **2018**, *14*, 97–104. [[CrossRef](#)]
5. Lima, P.; Steger, S.; Glade, T.; Tilch, N.; Schwarz, L.; Kociu, A. Landslide Susceptibility Mapping at National Scale: A First Attempt for Austria. In *Advancing Culture of Living with Landslides*; Springer International Publishing: Ljubljana, Slovenia, 2017; pp. 943–951.
6. Wu, Y.; Li, W.; Wang, Q.; Liu, Q.; Yang, D.; Xing, M.; Pei, Y.; Yan, S. Landslide susceptibility assessment using frequency ratio, statistical index and certainty factor models for the Gangu County, China. *Arab. J. Geosci.* **2016**, *9*, 84. [[CrossRef](#)]
7. Haque, U.; Blum, P.; da Silva, P.F.; Andersen, P.; Pilz, J.; Chalov, S.R.; Malet, J.-P.; Auflič, M.J.; Andres, N.; Poyiadji, E.; et al. Fatal landslides in Europe. *Landslides* **2016**, *13*, 1545–1554. [[CrossRef](#)]
8. Guzzetti, F.; Mondini, A.C.; Cardinali, M.; Fiorucci, F.; Santangelo, M.; Chang, K.-T. Landslide inventory maps: New tools for an old problem. *Earth-Sci. Rev.* **2012**, *112*, 42–66. [[CrossRef](#)]
9. Hong, H.; Pradhan, B.; Xu, C.; Tien Bui, D. Spatial prediction of landslide hazard at the Yihuang area (China) using two-class kernel logistic regression, alternating decision tree and support vector machines. *Catena* **2015**, *133*, 266–281. [[CrossRef](#)]
10. Tehrany, M.S.; Pradhan, B.; Jebur, M.N. Flood susceptibility analysis and its verification using a novel ensemble support vector machine and frequency ratio method. *Stoch. Environ. Res. Risk Assess.* **2015**, *29*, 1149–1165. [[CrossRef](#)]
11. Roccati, A.; Faccini, F.; Luino, F.; Ciampalini, A.; Turconi, L. Heavy Rainfall Triggering Shallow Landslides: A Susceptibility Assessment by a GIS-Approach in a Ligurian Apennine Catchment (Italy). *Water* **2019**, *11*, 605. [[CrossRef](#)]
12. Feizizadeh, B.; Jankowski, P.; Blaschke, T. A GIS based spatially-explicit sensitivity and uncertainty analysis approach for multi-criteria decision analysis. *Comput. Geosci.* **2014**, *64*, 81–95. [[CrossRef](#)] [[PubMed](#)]
13. Roodposhti, M.S.; Aryal, J.; Pradhan, B. A Novel Rule-based Approach In Mapping Landslide Susceptibility. *Sensors* **2019**, *19*, 2274. [[CrossRef](#)] [[PubMed](#)]
14. Pourghasemi, H.; Gayen, A.; Park, S.; Lee, C.-W.; Lee, S. Assessment of Landslide-Prone Areas and Their Zonation Using Logistic Regression, LogitBoost, and NaïveBayes Machine-Learning Algorithms. *Sustainability* **2018**, *10*, 3697. [[CrossRef](#)]
15. Van Westen, C.J. Remote Sensing and GIS for Natural Hazards Assessment and Disaster Risk Management. In *Treatise on Geomorphology*; Academic Press: San Diego, CA, USA, 2013; pp. 259–298.
16. Ghorbanzadeh, O.; Blaschke, T.; Aryal, J.; Gholaminia, K. A new GIS-based technique using an adaptive neuro-fuzzy inference system for land subsidence susceptibility mapping. *J. Spat. Sci.* **2018**, *63*, 1–17. [[CrossRef](#)]
17. Kienberger, S.; Lang, S.; Zeil, P. Spatial vulnerability units—Expert-based spatial modelling of socio-economic vulnerability in the Salzach catchment, Austria. *Nat. Hazards Earth Syst. Sci.* **2009**, *9*, 767–778. [[CrossRef](#)]
18. Khosravi, K.; Nohani, E.; Maroufinia, E.; Pourghasemi, H.R. A GIS-based flood susceptibility assessment and its mapping in Iran: A comparison between frequency ratio and weights-of-evidence bivariate statistical models with multi-criteria decision-making technique. *Nat. Hazards* **2016**, *83*, 947–987. [[CrossRef](#)]

19. Rahmati, O.; Pourghasemi, H.R.; Zeinivand, H. Flood susceptibility mapping using frequency ratio and weights-of-evidence models in the Golastan Province, Iran. *Geocarto Int.* **2015**, *31*, 42–70. [[CrossRef](#)]
20. Lee, S.; Pradhan, B. Landslide hazard mapping at Selangor, Malaysia using frequency ratio and logistic regression models. *Landslides* **2006**, *4*, 33–41. [[CrossRef](#)]
21. Rahmati, O.; Zeinivand, H.; Besharat, M. Flood hazard zoning in Yasooj region, Iran, using GIS and multi-criteria decision analysis. *Geomat. Nat. Hazards Risk* **2015**, *7*, 1000–1017. [[CrossRef](#)]
22. Ghorbanzadeh, O.; Feizizadeh, B.; Blaschke, T.; Khosravi, R. Spatially Explicit Sensitivity and Uncertainty Analysis for the landslide risk assessment of the Gas Pipeline Networks. In Proceedings of the 21st AGILE Conference on Geo-information Science, Lund, Sweden, 12–15 June 2018; pp. 1–7.
23. Nampak, H.; Pradhan, B.; Manap, M.A. Application of GIS based data driven evidential belief function model to predict groundwater potential zonation. *J. Hydrol.* **2014**, *513*, 283–300. [[CrossRef](#)]
24. Tehrany, M.S.; Pradhan, B.; Mansor, S.; Ahmad, N. Flood susceptibility assessment using GIS-based support vector machine model with different kernel types. *Catena* **2015**, *125*, 91–101. [[CrossRef](#)]
25. Chapi, K.; Singh, V.P.; Shirzadi, A.; Shahabi, H.; Bui, D.T.; Pham, B.T.; Khosravi, K. A novel hybrid artificial intelligence approach for flood susceptibility assessment. *Environ. Model. Softw.* **2017**, *95*, 229–245. [[CrossRef](#)]
26. Pradhan, B.; Lee, S.; Mansor, S.; Buchroithner, M.; Jamaluddin, N.; Khujaimah, Z. Utilization of optical remote sensing data and geographic information system tools for regional landslide hazard analysis by using binomial logistic regression model. *J. Appl. Remote Sens.* **2008**, *2*, 023542.
27. Felicísimo, Á.M.; Cuartero, A.; Remondo, J.; Quirós, E. Mapping landslide susceptibility with logistic regression, multiple adaptive regression splines, classification and regression trees, and maximum entropy methods: A comparative study. *Landslides* **2013**, *10*, 175–189. [[CrossRef](#)]
28. Hay, G.J.; Castilla, G. Geographic Object-Based Image Analysis (GEOBIA): A new name for a new discipline. In *Object-Based Image Analysis*; Springer: Berlin, Heidelberg, 2008; pp. 75–89.
29. Benz, U.C.; Hofmann, P.; Willhauck, G.; Lingenfelder, I.; Heynen, M. Multi-resolution, object-oriented fuzzy analysis of remote sensing data for GIS-ready information. *Isprs J. Photogramm. Remote Sens.* **2004**, *58*, 239–258. [[CrossRef](#)]
30. Blaschke, T.; Hay, G.J.; Kelly, M.; Lang, S.; Hofmann, P.; Addink, E.; Feitosa, R.Q.; Van der Meer, F.; Van der Werff, H.; Van Coillie, F. Geographic object-based image analysis—towards a new paradigm. *Isprs J. Photogramm. Remote Sens.* **2014**, *87*, 180–191. [[CrossRef](#)]
31. Lang, S.; Kienberger, S.; Tiede, D.; Hagenlocher, M.; Pernkopf, L. Geons—Domain-specific regionalization of space. *Cartogr. Geogr. Inf. Sci.* **2014**, *41*, 214–226. [[CrossRef](#)]
32. Costa, H.; Foody, G.M.; Boyd, D.S. Supervised methods of image segmentation accuracy assessment in land cover mapping. *Remote Sens. Environ.* **2018**, *205*, 338–351. [[CrossRef](#)]
33. Drăguț, L.; Csillik, O.; Eisank, C.; Tiede, D. Automated parameterisation for multi-scale image segmentation on multiple layers. *Isprs J. Photogramm. Remote Sens.* **2014**, *88*, 119–127. [[CrossRef](#)]
34. Shahabi, H.; Jarihani, B.; Tavakkoli Piralilou, S.; Chittleborough, D.; Avand, M.; Ghorbanzadeh, O. A Semi-Automated Object-Based Gully Networks Detection Using Different Machine Learning Models: A Case Study of Bowen Catchment, Queensland, Australia. *Sensors* **2019**, *19*, 4893. [[CrossRef](#)]
35. Ghorbanzadeh, O.; Blaschke, T.; Gholamnia, K.; Meena, S.R.; Tiede, D.; Aryal, J. Evaluation of Different Machine Learning Methods and Deep-Learning Convolutional Neural Networks for Landslide Detection. *Remote Sens.* **2019**, *11*, 196. [[CrossRef](#)]
36. Blaschke, T.; Piralilou, S.T. The near-decomposability paradigm re-interpreted for place-based GIS. In Proceedings of the 1st Workshop on Platial Analysis (PLATIAL'18), Heidelberg, Germany, 20–21 September 2018.
37. Yager, R.R.; Liu, L. *Classic Works of the Dempster-Shafer Theory of Belief Functions*; Springer: Berlin, Heidelberg, 2008; Volume 219.
38. Mezaal, M.; Pradhan, B.; Rizeei, H. Improving Landslide Detection from Airborne Laser Scanning Data Using Optimized Dempster–Shafer. *Remote Sens.* **2018**, *10*, 1029. [[CrossRef](#)]
39. Pham, B.T.; Bui, D.T.; Prakash, I.; Dholakia, M. Hybrid integration of Multilayer Perceptron Neural Networks and machine learning ensembles for landslide susceptibility assessment at Himalayan area (India) using GIS. *Catena* **2017**, *149*, 52–63. [[CrossRef](#)]
40. Tavakkoli Piralilou, S.; Shahabi, H.; Jarihani, B.; Ghorbanzadeh, O.; Blaschke, T.; Gholamnia, K.; Meena, S.R.; Aryal, J. Landslide Detection Using Multi-Scale Image Segmentation and Different Machine Learning Models in the Higher Himalayas. *Remote Sens.* **2019**, *11*, 2575. [[CrossRef](#)]

41. Petschko, H.; Brenning, A.; Bell, R.; Goetz, J.; Glade, T. Assessing the quality of landslide susceptibility maps—case study Lower Austria. *Nat. Hazards Earth Syst. Sci.* **2014**, *14*, 95–118. [[CrossRef](#)]
42. Tsangaratos, P.; Ilija, I. Comparison of a logistic regression and Naïve Bayes classifier in landslide susceptibility assessments: The influence of models complexity and training dataset size. *Catena* **2016**, *145*, 164–179. [[CrossRef](#)]
43. Ayalew, L.; Yamagishi, H. The application of GIS-based logistic regression for landslide susceptibility mapping in the Kakuda-Yahiko Mountains, Central Japan. *Geomorphology* **2005**, *65*, 15–31. [[CrossRef](#)]
44. Meena, S.R.; Ghorbanzadeh, O.; Blaschke, T. A Comparative Study of Statistics-Based Landslide Susceptibility Models: A Case Study of the Region Affected by the Gorkha Earthquake in Nepal. *Isprs Int. J. Geo-Inf.* **2019**, *8*, 94. [[CrossRef](#)]
45. Yalcin, A.; Bulut, F. Landslide susceptibility mapping using GIS and digital photogrammetric techniques: A case study from Ardesen (NE-Turkey). *Nat. Hazards* **2006**, *41*, 201–226. [[CrossRef](#)]
46. Bartelletti, C.; Giannecchini, R.; D’Amato Avanzi, G.; Galanti, Y.; Mazzali, A. The influence of geological–morphological and land use settings on shallow landslides in the Pogliaschina T. basin (northern Apennines, Italy). *J. Maps* **2017**, *13*, 142–152. [[CrossRef](#)]
47. Persichillo, M.G.; Bordoni, M.; Meisina, C. The role of land use changes in the distribution of shallow landslides. *Sci. Total Environ.* **2017**, *574*, 924–937. [[CrossRef](#)] [[PubMed](#)]
48. Cordeira, J.M.; Stock, J.; Dettinger, M.D.; Young, A.M.; Kalansky, J.F.; Ralph, F.M. A 142-year Climatology of Northern California Landslides and Atmospheric Rivers. *Bull. Am. Meteorol. Soc.* **2019**, *100*, 1499–1509. [[CrossRef](#)]
49. Dang, V.-H.; Dieu, T.B.; Tran, X.-L.; Hoang, N.-D. Hoang. Enhancing the accuracy of rainfall-induced landslide prediction along mountain roads with a GIS-based random forest classifier. *Bull. Eng. Geol. Environ.* **2018**, *78*, 2835–2849. [[CrossRef](#)]
50. Chen, W.; Pourghasemi, H.R.; Naghibi, S.A. A comparative study of landslide susceptibility maps produced using support vector machine with different kernel functions and entropy data mining models in China. *Bull. Eng. Geol. Environ.* **2017**, *77*, 647–664. [[CrossRef](#)]
51. Walter, V.; Fritsch, D. Automatic verification of GIS data using high resolution multispectral data. *Int. Arch. Photogramm. Remote Sens.* **1998**, *32*, 485–490.
52. Blaschke, T. Object based image analysis for remote sensing. *Isprs J. Photogramm. Remote Sens.* **2010**, *65*, 2–16. [[CrossRef](#)]
53. Hagenlocher, M.; Kienberger, S.; Lang, S.; Blaschke, T. Implications of spatial scales and reporting units for the spatial modelling of vulnerability to vector-borne diseases. *Gi_Forum* **2014**, *2014*, 197.
54. Tiede, D.; Lang, S.; Albrecht, F.; Holbling, D. Object-based Class Modeling for Cadastre-constrained Delineation of Geo-objects. *Photogramm. Eng. Remote Sens.* **2010**, *76*, 193–202. [[CrossRef](#)]
55. Drăguț, L.; Tiede, D.; Levick, S.R. ESP: A tool to estimate scale parameter for multiresolution image segmentation of remotely sensed data. *Int. J. Geogr. Inf. Sci.* **2010**, *24*, 859–871. [[CrossRef](#)]
56. Foley, B.G. A Dempster-Shafer Method for Multi-Sensor Fusion. 2012.
57. Feizizadeh, B.; Blaschke, T.; Nazmfar, H. GIS-based ordered weighted averaging and Dempster–Shafer methods for landslide susceptibility mapping in the Urmia Lake Basin, Iran. *Int. J. Digit. Earth* **2014**, *7*, 688–708. [[CrossRef](#)]
58. Martin, R.; Zhang, J.; Liu, C. Dempster–Shafer theory and statistical inference with weak beliefs. *Stat. Sci.* **2010**, *25*, 72–87. [[CrossRef](#)]
59. Eastman, J. *IDRISI Selva: Guide to GIS and Image Processing*; Clark Laboratories, Clark University: Worcester, MA, USA, 2012.
60. Feizizadeh, B. A Novel Approach of Fuzzy Dempster–Shafer Theory for Spatial Uncertainty Analysis and Accuracy Assessment of Object-Based Image Classification. *IEEE Geosci. Remote Sens. Lett.* **2018**, *15*, 18–22. [[CrossRef](#)]
61. Baraldi, P.; Zio, E. A comparison between probabilistic and dempster-shafer theory approaches to model uncertainty analysis in the performance assessment of radioactive waste repositories. *Risk Anal. Int. J.* **2010**, *30*, 1139–1156. [[CrossRef](#)]
62. Rottensteiner, F.; Trinder, J.; Clode, S.; Kubik, K. Using the Dempster–Shafer method for the fusion of LIDAR data and multi-spectral images for building detection. *Inf. Fusion* **2005**, *6*, 283–300. [[CrossRef](#)]

63. Ghorbanzadeh, O.; Valizadeh Kamran, K.; Blaschke, T.; Aryal, J.; Naboureh, A.; Einali, J.; Bian, J. Spatial Prediction of Wildfire Susceptibility Using Field Survey GPS Data and Machine Learning Approaches. *Fire* **2019**, *2*, 43. [[CrossRef](#)]
64. Ghorbanzadeh, O.; Rostamzadeh, H.; Blaschke, T.; Gholaminia, K.; Aryal, J. A new GIS-based data mining technique using an adaptive neuro-fuzzy inference system (ANFIS) and k-fold cross-validation approach for land subsidence susceptibility mapping. *Nat. Hazards* **2018**, *94*, 497–517. [[CrossRef](#)]
65. Ghorbanzadeh, O.; Feizizadeh, B.; Blaschke, T. Multi-criteria risk evaluation by integrating an analytical network process approach into GIS-based sensitivity and uncertainty analyses. *Geomat. Nat. Hazards Risk* **2018**, *9*, 127–151. [[CrossRef](#)]



© 2019 by the authors. Licensee MDPI, Basel, Switzerland. This article is an open access article distributed under the terms and conditions of the Creative Commons Attribution (CC BY) license (<http://creativecommons.org/licenses/by/4.0/>).